Molecular Recognition – Allosterism Generated by Weak Host–Guest Interactions in Molecular Rectangles

James D. Crowley,[a] Ian M. Steele,[a] and Brice Bosnich*[a]

Keywords: Host–guest systems / Molecular recognition / Allosterism / Self-assembly / Supramolecular chemistry

Two metal-based molecular rectangles that bear two identical binding sites form 1:2 host–guest adducts with a pair of analogous planar Pt^{2+} complexes. The larger of the two guests shows no binding allosterism with either of the two rectangles, but substantial positive allosterism is observed when the smaller guest binds to the rectangles. It is proposed that the smaller guest is better accommodated in the binding sites of the receptor and that this leads to allosterism. Various experiments, including ^{1}H NOESY spectroscopy, support the supposition that the smaller guest is better incarcerated in the receptors.

1. Introduction

Allosterism is commonly deployed by biological systems for controlling and regulating function. In these systems, the binding of a substrate usually engenders conformational or other changes in the receptor so that the subsequent binding of the same substrate at other identical sites is either of enhanced or of decreased stability. The mechanisms that generate positive or negative allosterism are subtle, and they are poorly understood in complicated systems. There have been numerous model systems developed,[1] starting with the classical experiments of Rebek.[2] Rebek devised several allosteric systems, including **1**.

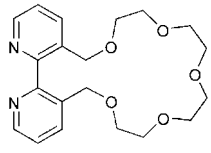

1

The bipyridyl-bound complex [(**1**)W(CO)$_4$] is a (kinetically) stable molecule. Using a U-tube where water is separated by CH_2Cl_2, it was found that the free ligand **1** transported K^+ in preference to Na^+, but that the tungsten complex caused these preferences to be reversed. It was assumed that the transport preference is related to the stability of the alkali ion in the crown-ether site. The bipyridyl that binds to the tungsten generates a different preferred conformation for the crown ether from that adopted by the free ligand **1**. Thus, the tungsten bound to the bipyridyl is mechanically coupled to the crown ether site, leading to different binding affinities of the alkali metals. Following from this work, there have been numerous examples of allosterism involving dinuclear ligands, where the insertion of a metal into one site leads to increased or diminished binding of a second metal in the other site.[1] Some of these systems have been especially sophisticated, some involve allosteric control of catalysis.[1] In some respects, generating allosterism by homo- or heterotopic coordination of metals has a well-understood logic, which relies on the positioning of coordinating ligands for binding to metals with commensurate stereochemical demands. These aspects are cogently presented in Kramer's review.[1]

The next level of complexity in synthetic modeling was in deploying weak (directional) hydrogen bonding for mechanical coupling. The first example of allosterism generated by hydrogen bonding was reported by Hunter[3] who synthesized a host with two identical hydrogen bonding sites for the guest, quinone. In $CHCl_3$ solution, positive allosterism was observed for the two homotopic sites of the host. The allosterism was modest; the successive constants were $K_1 = 14\ M^{-1}$ and $K_2 = 28\ M^{-1}$. Later, a similar hydrogen-bonding homoditopic receptor was found to give positive allosterism for a single guest.[4] More recently, a carefully designed homoditopic system was found capable of giving high positive allosterism for a variety of guests.[5] Differences of 33:1 between the two constants were reported.

As far as we are aware, no examples of allosterism involving weak, poorly directional forces, such as π–π interactions, have been reported.[1e] This paper reports cases where weak molecular recognition forces lead to positive allosterism.

[a] Department of Chemistry, The University of Chicago, 5735 South Ellis Avenue, Chicago, Illinois 60637, USA
E-mail: bos5@uchicago.edu
Fax: +1-773-702-0805

Supporting information for this article is available on the WWW under http://www.eurjic.org or from the author.

2. Receptors and Guests

Molecular rectangles bearing two identical sites were used for investigating allosterism. The molecular cleft **2** is joined by the linkers **3** or **4** to give the molecular rectangles as shown schematically in Equation (1). The three potential metal-containing guests, **5**, **6**, and **7**, were investigated in order to study allosterism. With receptor **2**, both of the guests **5** and **6** form stable 1:1 host–guest complexes in solution.[6,7]

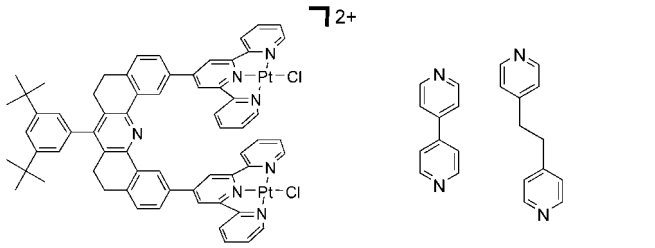

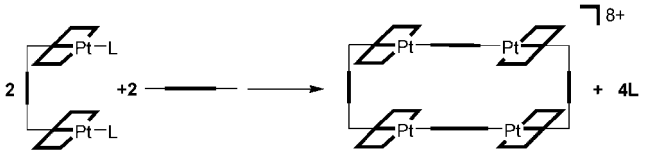

(1)

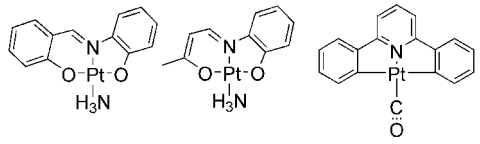

Crystal structures and NOE experiments[6,7] show that the guests **5** and **6** lie within the molecular cleft of **2**. In the solid state, and probably also in solution, the guests **5** and **6** engage in weak Pt–Pt interaction with the receptor **2**. The maximum separation between the face-to-face terpy-Pt-X units of receptor **2** is about 7.2 Å. The crystal structure shows that this interplanar separation is contracted to 6.557 Å in order to accommodate guest **5** in **2**.[6] This contraction is achieved by the concerted rotation of the terpy-Pt-X units about the spacer unit as shown in Scheme 1.

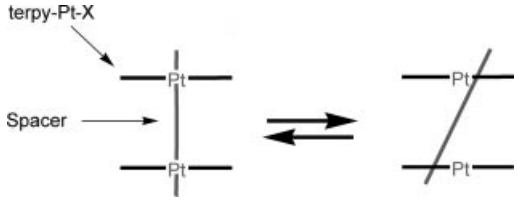

Scheme 1.

Addition of the guests **5** or **6** to solutions of the molecular rectangles will lead to stepwise incarceration of the guests into the molecular clefts. Upon the addition of the first guest, the terpy-Pt-linker unit separation is likely to contract to accommodate the guest. When this happens, the other terpy-Pt-linker unit separation is also likely to contract, because the sites are mechanically coupled by the linkers **3** and **4**. Linker **4** is less rigid than linker **3** and this may lead to less rigid mechanical coupling of the sites. Thus it is conceivable that after the insertion of one guest into a site, the other site may become better organized to accept the second guest because of conformational changes induced by the first adduct formation. If this is the case, then positive allosterism might be observed in host–guest adducts of the rectangles. The reason for including **7**[8] as a guest will become apparent later.

The preparation of the receptor ligand in **2** has been described elsewhere[9] as was the preparation of **5**,[6] **6**,[7] and **7**.[8] Because the reactions of Pt^{2+} complexes are usually kinetically slow, the procedure outlined in Scheme 2 was used for incorporating Pt^{2+} into the two terpy sites of the ligand. The rate of Pt^{2+} incorporation is enhanced by the trans-effect of the olefins and by the fact that presumably labile acetone ligands are being substituted. The reactions are carried out under anhydrous conditions to avoid the formation of nonlabile hydroxo complexes. Solutions of the dipyridine compound **9** and of the two rectangles are kinetically stable at room temperature and below. This behavior contrasts with that of the analogous Pd^{2+} compounds,[10] which are kinetically labile in solution at room temperature. The two rectangles in dimethyl formamide (DMF) solutions give ESI-MS spectra[11] that are devoid of fragmentation and show ion peaks that are consistent with the proposed structures, which, in turn, are confirmed by the peak isotopic distribution of the 2+ ions (Supporting Information). Furthermore, the ^1H NMR spectra of the two rectangles are in full accord with the proposed structures (Supporting Information). There seems little doubt that the molecular rectangles have been correctly identified.

3. Host–Guest Formation

All of the host–guest adduct investigations were carried out in [D_7]DMF solutions at 60 °C. DMF was used because it is a poorly coordinating solvent, and, at 60 °C in this solvent, all of the ^1H NMR spectral peaks are sharp for both the host and the guest. By following the change in chemical shift for certain protons as a function of the mol ratio of host to guest, the stoichiometry of the binding and the binding constants were determined.[12]

As expected, either guest, **5** or **6**, formed 1:1 host–guest adducts with receptor **9** (see Figure 6). The stability constants are listed in Table 1. The smaller value of the stability constant for the **9**–**6** adduct may be related to the smaller π-surface of guest **6**. For both host–guest complexes, complexation-induced chemical shifts are observed for the (internal) H_e but not for the (outer) H_d protons (see Scheme 2), indicating that the guest resides within the molecular cleft. Upon host–guest formation, the color changes

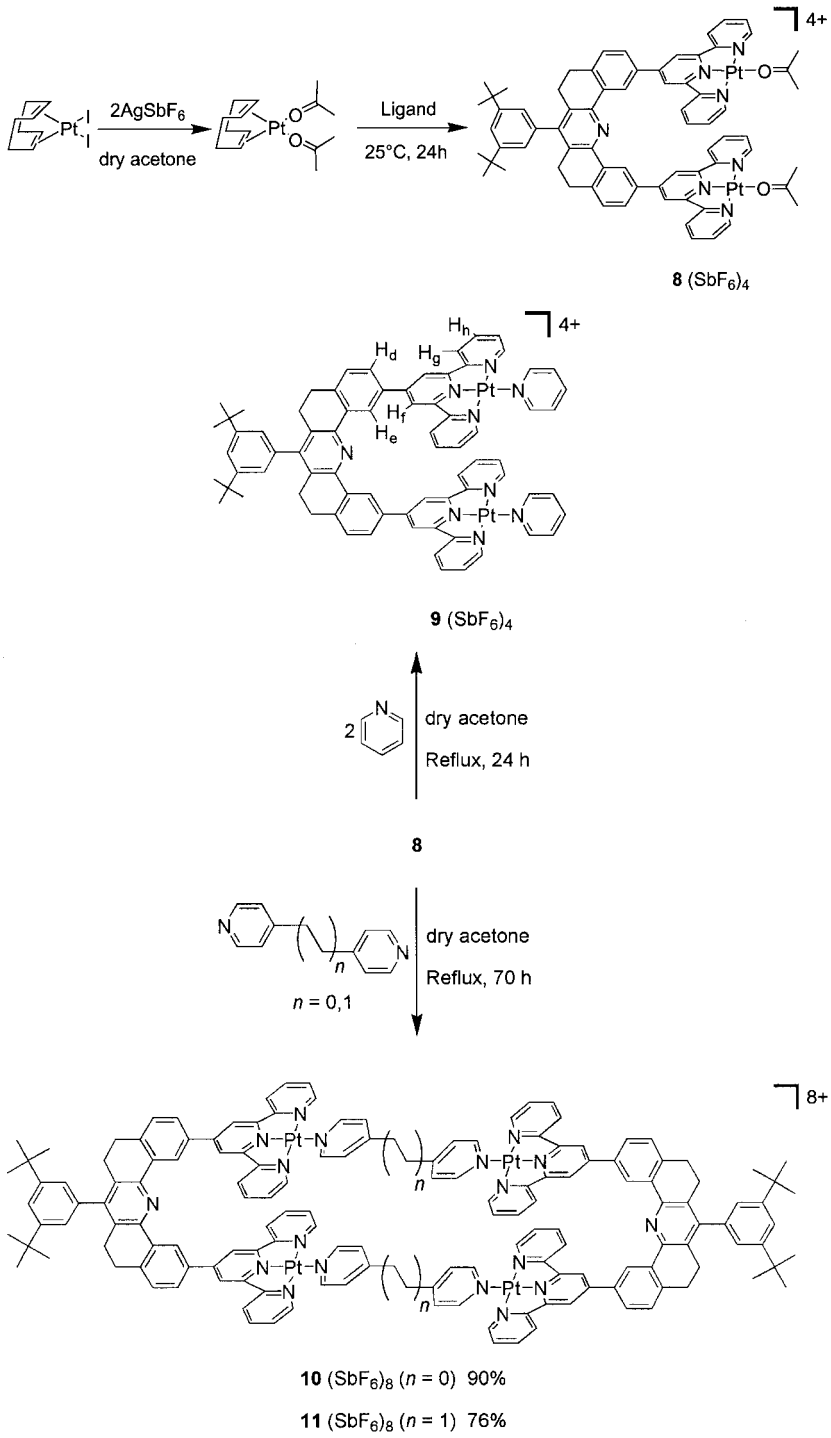

Scheme 2.

to deep red from the light yellow of the components (see Figure 5). The ESI-MS of the host–guest adducts gives peaks for the free receptor, in addition, strong peaks are observed for the 1:1 host–guest adducts formed by **9** with **5** (see Figure 7) and with **6**.

The stabilities of the host–guest adducts **9**–**5** and **9**–**6** should be related in some respects to the first association constants for the two molecular rectangles **10** and **11** (Scheme 2). At 60 °C in [D_7]DMF solution, a 1:2 host–guest complex was found to form between the molecular rectangle **10** and the guest **5** (see Figure 9). As expected, host–guest formation is signaled by the appearance of a deep red color (see Figure 8). ESI-MS of the host–guest adduct, **10**–(**5**)$_2$, provides peaks for the free rectangle, for the receptor with one guest associated, and for the 1:2 host–guest adduct (see Figure 10). Similar ESI-MS data are observed for all rectangle adducts listed in Table 1, and in all cases, host–guest formation is signaled by the appearance

of red-colored solutions. The two statistically adjusted microscopic stability constants[13] for the adduct are listed in Table 1 together with the ratio of the stability constants, K_2/K_1. No allosterism is observed for this system: the two constants are the same within experimental error. The absence of allosterism for rectangle **10** could be connected with the rigidity of the linker, which may hinder appropriate mechanical coupling between the two sites. Rectangle **11** has a more flexible linker, and this circumstance might allow favorable conformational adjustment at the binding sites. The two microscopic stability constants for the host–guest adduct **11**–(**5**)$_2$ are listed in Table 1. Again, no allosterism is observed within experimental error. Interestingly, the association constants for the adducts **10**–(**5**)$_2$ and **11**–(**5**)$_2$ are the same within experimental error. The absence of allosterism in either of these cases might suggest that the structure of the guest may influence whether or not allosterism is observed. It was supposed that a smaller guest such as **6** might fit better into the molecular clefts of the rectangles, and, as a consequence, better mechanical coupling between the two binding sites may ensue.

The pairs of stability constants for the 1:2 host–guest adducts **10**–(**6**)$_2$ and **11**–(**6**)$_2$ are given in Table 1. Positive allosterism is observed for both adducts, the **11**–(**6**)$_2$ system having the larger cooperative enhancement.

Table 1. Microscopic stability constants (M^{-1}) for host–guest formation in [D_7]DMF at 60 °C.

Adduct	Host–Guest Stoichiometry	K_1 [M^{-1}]	K_2 [M^{-1}]	Ratio K_2/K_1
9–**5**	1:1	3760 ± 600	–	–
9–**6**	1:1	1160 ± 200	–	–
10–(**5**)$_2$	1:2	4100 ± 200	4200 ± 100	1.02
11–(**5**)$_2$	1:2	3800 ± 300	4400 ± 100	1.15
10–(**6**)$_2$	1:2	1450 ± 200	5200 ± 400	3.58
11–(**6**)$_2$	1:2	1250 ± 200	5600 ± 400	4.58

The free energy associated with the first stability constant (K_1) of the adducts **10**–(**6**)$_2$ and **11**–(**6**)$_2$ incorporates the free energy of the conformational rearrangement that leads to allosterism. Thus one might expect that the stability constant for the analogous uncoupled adduct, **9**–**6**, would be larger than the first constants for **10**–(**6**)$_2$ and **11**–(**6**)$_2$. The formation constants for the **9**–**6** adduct and the first association constants (K_1) for the **10**–(**6**)$_2$ and **11**–(**6**)$_2$ adducts are essentially the same (Table 1). Similarly, even though the adducts **10**–(**5**)$_2$ and **11**–(**5**)$_2$ show no allosterism, their first constant (K_1) is essentially the same as the constant (K) found for the 1:1 adduct, **9**–**5**. We discuss these observations later but we can provide no plausible explanation for the results.

The fact that the 1:2 adducts **10**–(**5**)$_2$ and **11**–(**5**)$_2$ show no allosterism whereas the 1:2 adducts **10**–(**6**)$_2$ and **11**–(**6**)$_2$ do may, as we have suggested, be connected with the ability of the receptors to accommodate the smaller guest **6**. ^{1}H NOE experiments suggest that this may be the case.

4. ^{1}H NOE Experiments on the Host–Guest Adducts, 10–(5)$_2$ and 10–(6)$_2$

The ^{1}H NOESY experiments[14] were carried out in [D_7]DMF solutions at 60 °C. The results for the **10**–(**5**)$_2$ and **10**–(**6**)$_2$ host–guest adducts are illustrated in Figure 1 and Figure 2, respectively. Since the rectangles have symmetry operations that interchange the protons H_e and H_d with the corresponding protons of the spacer, the symmetry-related protons are not shown. It will be seen that the two systems (Figures 1 and 2) show different ^{1}H NOESY cross-peaks, but both spectra clearly demonstrate that the guests reside only within the molecular clefts. The two guests **5** within rectangle **10** show cross-peaks between the protons, H_e and H_k, of the rectangle and the "back" (H_s, H_r, H_q, H_p and H_o) and "front" (H_v, NH_3) protons of the guest. The guests are shown in one pair of orientations, but the cross-peaks clearly indicate that several orientations of the guest within the clefts exist for the **10**–(**5**)$_2$ adduct. For the 1:2 host–guest adduct, **10**–(**6**)$_2$, the ^{1}H NOESY data clearly show that the guests exist in one preferred orientation as illustrated in Figure 2, where the ammine ligands of the guests point at the 4,4′-dipyridyl linkers.

It will be noted that for both adducts (Figures 1 and 2) some protons of the guest show no cross-peaks with the host. Given that NOE cross-peaks are generally observed at distances of less than about 3.5 Å,[14] the orientation of the guests in the rectangle **10** is roughly as shown in Figure 1, where the *ortho*-amino phenolate residue probably resides, to some extent, outside of the cleft. The several mutual orientations of the two guests within the rectangular receptor are probably interchanged by intermolecular exchange because scale molecular models suggest that the receptor site does not appear to be large enough to allow for intramolecular rotation of the guest.

Because of the interaction of the *ortho*-protons of the pyridine ligands of the linker with those of the flanking pyridyl ligands of the terpy-Pt unit, the pyridine ligand planes of the linker are expected to lie roughly perpendicular to the terpy-Pt units. The barrier to rotation of the linker pyridine ligands cannot be high, because, even at –90 °C in acetone solution, rapid rotation of the pyridine ligands occurs on a ^{1}H NMR time scale (500 MHz).[10] At 60 °C in [D_7]DMF, the 1:2 host–guest adducts also show rapid rotation of the linker pyridine ligands, but the preferred orientation of the pyridine planes is likely to be perpendicular to the terpy-Pt^{2+} plane. Scale molecular models indicate that when the planes of the linker pyridine ligands lie roughly perpendicular to the terpy-Pt plane, the guests, especially **5**, cannot be fully accommodated within the molecular clefts of the rectangles. It is probable that guest incarceration does not provide sufficient energy to cause the planes of the linker pyridine groups to approach planarity with the terpy-Pt units to open the cleft cavity. Thus, we suggest that the pyridine ligands of the linkers are the main steric impediment to complete incarceration of guest **5**. As shown in Figure 2, guest **6** has only one predominant orientation within the host. Presumably the smaller size of **6** relative to **5** al-

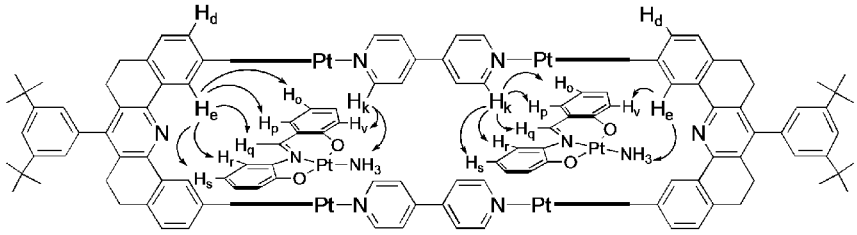

Figure 1. Cross-peaks observed for the 1:2 host–guest adduct **10**–(**5**)$_2$ in [D$_7$]DMF at 60 °C.

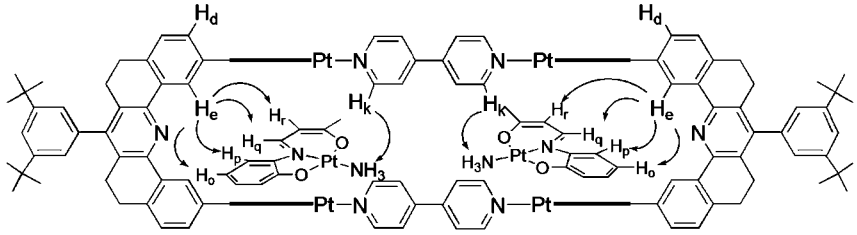

Figure 2. Cross-peaks observed for the 1:2 host–guest adduct **10**–(**6**)$_2$ in [D$_7$]DMF at 60 °C. Possible cross-peaks with the guest methyl group were not investigated.

lows the former to fit better within the cleft. As for the case of the adduct between **2** and **5**,[6] where the guest also has a single orientation and the crystal structure reveals Pt–Pt interaction, it is suggested that Pt–Pt interaction exists for the 1:2 adduct **10**–(**6**)$_2$. These observations suggest that the observed allosterism may depend on how well the guests are accommodated within the hosts, and Pt–Pt interaction may possibly fix the orientation of the guest, which may also contribute to favorable mechanical coupling. The arguments given above depend on the assumption that the disposition of the linker pyridine groups prevents the full accommodation of guests having the dimensions of **5** or larger. Since the barrier to pyridine ligand rotation is unknown, it is possible to argue that the guests could cause the linker pyridine groups to rotate so as to accommodate the guest. This postulate implies that the free energy of host–guest formation is sufficient to overcome the major part of the linker pyridine rotational barrier. In order to explore this matter further, we have studied the host–guest behavior of the much larger guest **7**[8,15] with **10**.

5. Host–Guest Formation of 10 with 7

The receptor **2** forms a bright red 1:2 host–guest complex with the guest **7**, where one guest lies within the molecular cleft and the other guest lies on the outer faces of the terpy-Pt-Cl units.[15] The Pd^{2+} rectangle analogous to **10** forms a red 1:4 host–guest complex with 9-methylanthracene (**12**).[16] In this case, two of the guests lie in the two molecular clefts, and the other two guests are associated with the outer faces of the terpy-Pd-linker units. In [D$_7$]DMF at 60 °C, addition of **7** to the rectangular receptor **10** causes a slightly visible change in color, and ESI-MS data show only ions corresponding to the receptor (Supporting Information). ^{1}H NMR spectral shift titration indicates that a 1:4 host–guest complex is formed (Supporting Information). Inspection of the host protons whose chemical shifts change upon host–guest formation suggests that guest **7** does not occupy the molecular clefts of receptor **10**. This was confirmed by ^{1}H NOESY spectra at 60 °C in [D$_7$]DMF, where only the receptor protons H$_d$ and H$_k$ (but not H$_e$)

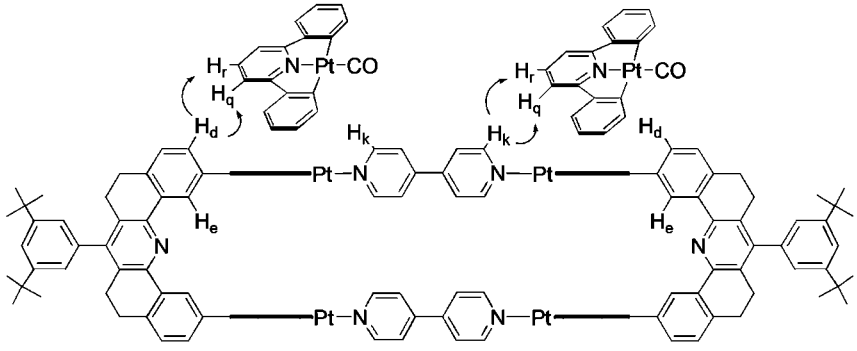

Figure 3. Cross-peaks observed for the 1:4 host–guest adduct **10**–(**7**)$_4$ in [D$_7$]DMF at 60 °C. Only two guests are shown, one for each of the two orientations.

have cross-peaks to the protons of the guest (Figure 3). The ^{1}H NMR spectrum indicates that the 4,4′-dipyridyl linkers are rapidly rotating so that both of the protons adjacent to the pyridine nitrogen atoms have cross-peaks with the guest. The observed cross-peaks (Figure 3) indicate that the guest adopts two orientations, as evidenced by the interaction of both H_d and H_k with H_r and H_q. Since a 1:4 host–guest complex is formed, it is not possible to obtain the four stability constants, but it is clear that guest **7** does not occupy the molecular clefts of **10** to any significant degree. These data support our supposition that the pyridine ligands of the linkers restrict access to the molecular cleft and that it is possible that a guest of the size of **5** may have difficulty in being fully incarcerated in the clefts. As a consequence, it may be that in such circumstances there is only weak mechanical coupling between the sites.

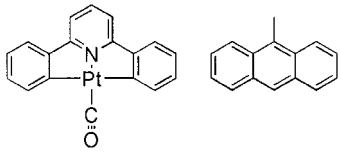

7 **12**

6. X-ray Diffraction Studies

We have attempted to obtain suitable crystals for X-ray diffraction from the host–guest complexes formed by the molecular rectangles **10** and **11** and the two guests **5** and **6** as well as the guest-free rectangles **10** and **11**. Except for crystals formed by the host–guest adduct **10**–(**5**)$_2$, none of the other solids diffracted in a manner suitable for structure determination. The crystals of **10**–(**5**)$_2$ were formed from methyl ethyl ketone by methanol diffusion. The crystals diffracted but they were disordered, and only an outline of the molecular rectangle structure could be obtained. The crystallographic data are listed in Table 2, and the derived structure is shown in Figure 4. The solvent molecules, the SbF_6^- counter ions, the guest molecules, and the di-*tert*-butyl phenyl substituents on the spacers are very disordered and are not shown in Figure 4.

The positions of the guest molecules were indicated by the electron density of the Pt^{2+} ions, which appear in the two molecular clefts and on the outside faces of the four terpy-Pt-linker units of the rectangle. The disorder may arise from this multiple occupancy of these sites. Attempts to crystallize the **10**–(**5**)$_2$ with two extra equivalents of **5** in the hope of occupying all of the guest sites with molecules of **5** failed.

The molecular rectangle is in a *meso* conformation with one spacer in the *R*,*R* and the other in the *S*,*S* configuration. The bonding of the linkers to the Pt^{2+} atoms is not ideal, and the 4,4′-dipyridyl linkers are buckled in order to link to the Pt^{2+} atoms (see lower structure in Figure 4). Presumably this linker strain would be relieved for the rectangle **11** that carries the more flexible 4,4′-dipyridylethane (**4**) linker. The planes of the pyridine groups of the linkers are essentially perpendicular to the plane of the terpy-Pt^{2+} units, a geometry that was inferred from the modeling of the rectangles. Adjacent planes of the terpy-Pt^{2+} units of each cleft are nearly parallel to each other, and the interplanar separation is about 6.9 Å. The "width" of a pyridine (from hydrogen to corresponding hydrogen) is about

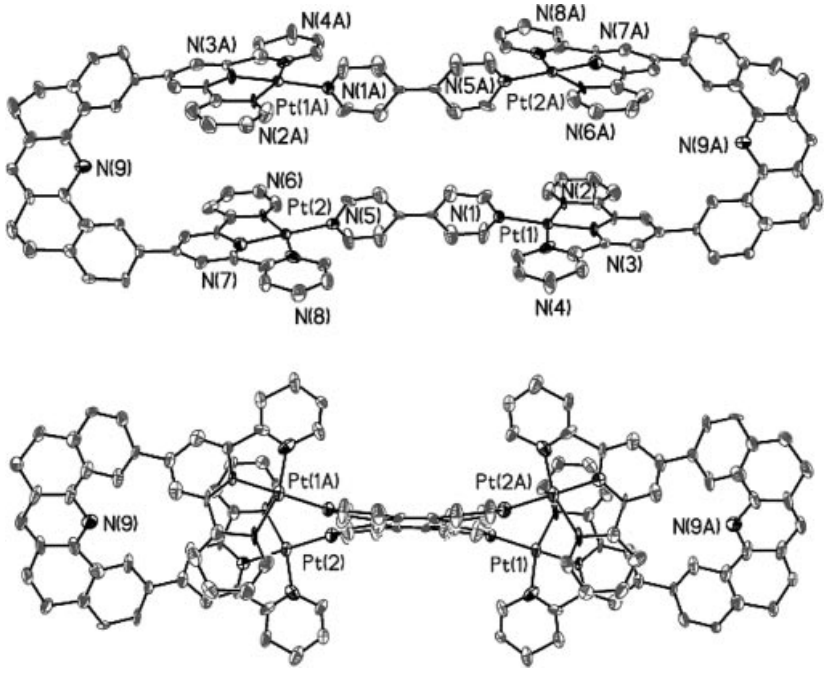

Figure 4. ORTEP diagrams of the "core" of the molecular rectangle. Above, a "side" view, below a "top" view. The disordered guest molecules **5**, the *tert*-butyl-containing phenyl rings of the spacer, the SbF_6^- ions, and the solvents of crystallization have been omitted for clarity. The thermal ellipsoids are shown at 50% probability.

Table 2. Crystallographic data for the host–guest adduct formed from **10** and **5**.

Compound	**10**–(**5**)$_2$
Formula	$C_{67}N_9Pt_4$ + 3Sb +10F (as refined)
Formula weight	2266.37 (as refined)
space group	$P\bar{1}$
a [Å]	13.886(10)
b [Å]	16.026(11)
c [Å]	35.67(3)
α [deg]	77.126(12)
β, [deg]	85.113(16)
γ, [deg]	67.426(12)
V [Å]^3	7146(9)
Z	2
cryst. size, color, habit	0.20 × 0.15 × 0.15 mm, red, brick
D(calc) [g cm^{-3}]	1.053
μ [mm^{-1}]	4.493
temp [K]	100(5)
Wavelength [Å]	0.71073 (Mo-K_α)
$R(F)$, %[a]	14.84
$R(wF^2)$, %[a]	40.25

[a] Quantity minimized = $R(wF^2) = \Sigma[w(F_o^2 - F_c^2)^2]/\Sigma[(wF_o^2)^2]^{1/2}$; $R = \Sigma\Delta/\Sigma(F_o)$, $\Delta = (F_o - F_c)$; $w = 1/[\sigma^2(F_o^2) + (aP)^2 + bP]$, $P = [2F_c^2 + \mathrm{Max}(F_o, 0)]/3$.

5 Å. Thus, the corresponding pyridine groups of neighboring linkers have nearest approach distances of about 1.9 Å if the pyridine groups of different linkers are aligned as is nearly the case (Figure 4). A separation of this magnitude will not allow a guest to reside between pyridine groups and would not allow a large guest such as **7** to fit into the molecular cleft. The interplanar separation of the terpy-Pt^{2+} units is uncharacteristically large. Usually, this separation is 6.8 Å or less,[17] and the separation in the present system is at the outer limits of π–π stacking distances. There does not seem to be any steric impediment to the contraction of the parallel terpy-Pt^{2+} units to a separation of 6.7 Å. A smaller guest such as **6** may cause this interplanar separation contract more.

7. Discussion

Understanding the origins of allosterism in multimetallic ligand systems and even in hosts bearing hydrogen bonds is relatively simple in outline. This is so for the former because the coordination geometries of metals and the requirements of the ligands are understood. For the latter systems, the geometry of hydrogen bonding with given substrates is usually understood, and, consequently, there are plausible rationalizations that can be advanced on the basis of the directions of the hydrogen bonds. With systems that rely on weak, poorly directional π–π or similar interactions, attempts to rationalize the allosterism are more difficult. This is the case even for the present rectangles that appear to provide a simple mechanism for mechanical coupling between sites. Whereas substantial positive allosterism was observed for the 1:2 host–guest complexes **10**–(**6**)$_2$ (K_2/K_1 = 3.58) and **11**–(**6**)$_2$ (K_2/K_1 = 4.58), the energy differences between the two constants are small. For the former, the free energy difference is 0.65 kcal mol^{-1}, and for the latter the difference is 1.01 kcal mol^{-1}. It is therefore difficult to ascribe these small energy differences to specific interactions of conformational changes for complicated hosts such as the present rectangles. Despite these difficulties, work on allosterism generated by weak interactions is important because biological systems rely on the concerted orchestration of these weak forces.

Experimental Section

Procedures: All reagents were obtained from commercial suppliers and were used without further purification. All reactions were performed under argon, unless otherwise specified. Electronic absorption spectra were obtained with a Perkin–Elmer Lambda 6 UV/Vis spectrophotometer. Elemental analyses were performed by Desert Analytics, Inc., Tucson, Arizona. ^{1}H and ^{13}C NMR spectra were recorded with a Bruker DRX500 Fourier transform spectrometer at 300 K, unless specified otherwise. Proton and carbon chemical shifts, *δ*, are reported in ppm, referenced to TMS. Coupling constants, *J*, are reported in Hertz. APCI-MS and ESI-MS were obtained with an Agilent 1100 MSD LC-MS. Acetonitrile was dried with CaH_2, tetrahydrofuran (THF) was dried with potassium/benzophenone ketyl, diethyl ether (Et_2O) was dried with sodium/benzophenone ketyl, dichloromethane (CH_2Cl_2) was dried with CaH_2, and triethylamine (TEA) was dried with CaH_2. Thin-layer chromatography was carried out using precoated silica gel (Whatman PE SIL G/UV) or precoated aluminum oxide (J. T. Baker, aluminum oxide IB-F). Silica gel 60 Å (Merck, 230–400 mesh) and aluminum oxide 58 Å (either activated, basic, Brockman I or activated, neutral, Brockman I) were used for chromatography as indicated. Celite is J.T. Baker Celite 503. The receptor ligand **L**[9] and the guests **5**,[6] **6**,[7] and **7**[8] were prepared by methods previously described. The linkers 4, 4′-dipyridyl (**3**) and 4, 4′-dipyridylethane (**4**), and [(COD)PtI_2] were obtained from the Sigma–Aldrich Chemical Co. and were used without further purification.

[$LPt_2(Py)_2$][SbF_6]$_4$, Receptor 9: The following procedure must be performed with rigorous exclusion of water. A dried 25-mL flask was charged with $AgSbF_6$ (0.185 g, 0.538 mmol) dissolved in anhydrous acetone (10 mL). To a suspension of [(COD)PtI_2] (0.150 g, 0.269 mmol) in dry acetone (5 mL) was added the colorless solution of the silver salt. Upon addition, the COD complex rapidly dissolved and AgI precipitated. The reaction was stirred for 1 h at room temperature, with brief sonication midway through this period. The AgI was removed by Schlenk filtration through a fine-porosity frit under argon. The receptor ligand **L** (0.126 g, 0.135 mmol) was added to the clear solution. The ligand dissolved rapidly, and the color of the solution changed to orange-yellow. The reaction was stirred at room temperature for 24 h, during which time the color became less orange. Pyridine (0.026 g, 0.028 mL, 0.330 mmol) was added to the solution, and the reaction mixture was heated at reflux (70 °C). The mixture was stirred at this temperature for 24 h. The solvent was then removed under reduced pressure to yield a yellow solid, which was slurried in cold methanol and recovered by filtration. It was washed with cold methanol (1 × 5 mL), ether (1 × 5 mL), and pentane (2 × 5 mL), then dissolved in acetone (5 mL) and filtered through Celite. The product was crystallized by vapor diffusion of diethyl ether into the acetone solution. The receptor **9** was recovered by filtration and was washed with diethyl ether (1 × 5 mL) followed by pentane (2 × 3 mL). Yield = 0.280 g (86%). ^{1}H NMR ([D_6]acetone, 27 °C, 500 MHz): *δ* = 1.41 (s, 18 H), 2.86 (t, *J* = 6.55 Hz, 4 H), 3.16 (t, *J* = 6.75 Hz, 4 H), 7.23 (d, *J* = 1.68 Hz, 2 H), 7.65–7.69 (m, 3 H),

7.93 (t, J = 6.79 Hz, 4 H), 8.05–8.08 (m, 4 H), 8.15 (d, J = 7.55 Hz, 4 H), 8.48 (t, J = 7.88 Hz, 2 H), 8.57 (t, J = 7.65 Hz, 4 H), 8.89 (d, J = 7.75 Hz, 8 H), 9.17–9.19 (m, 4 H), 9.32 (d, J = 5.09 Hz, 4 H) ppm. $C_{75}H_{65}F_{24}N_9Pt_2Sb_4$ (2425.54): calcd. C 37.14, H 2.70, N 5.20; found C 37.33, H 2.94, N 4.96. ESI-MS: a series of peaks were observed that were consistent with $[M - n(SbF_6)]^{n+}$ (n = 1–4): for example, 370.2 [**9** – 4(SbF_6)]$^{4+}$, 572.3 [**9** – 3(SbF_6)]$^{3+}$, 976.0 [**9** – 2(SbF_6)]$^{2+}$, 2188.9 [**9** – 1(SbF_6)]$^{+}$.

Pt Molecular Rectangle Formed with 4,4′-Dipyridyl (10): The following procedure must be performed with rigorous exclusion of water. A dried 25-mL flask was charged with $AgSbF_6$ (0.185 g, 0.538 mmol) dissolved in anhydrous acetone (10 mL). To a suspension of [(COD)PtI_2] (0.150 g, 0.269 mmol) in dry acetone (5 mL) was added the colorless solution of the silver salt. Upon addition, the COD complex rapidly dissolved and AgI precipitated. The reaction was stirred for 1 h at room temperature, with brief sonication midway through this period. The AgI was removed by Schlenk filtration under argon. The receptor ligand **L** (0.126 g, 0.135 mmol) was added to the clear solution. The ligand dissolved rapidly, and the color of the solution changed to orange-yellow. The reaction was stirred at room temperature for 24 h, during which time the color became less orange. The linker 4,4′-dipyridyl (0.021, 0.135 mmol) was added to the solution, and the reaction mixture was heated at reflux (70 °C). The mixture was stirred at this temperature for 2 d. At the end of this period, the solvent was removed under reduced pressure to yield a yellow solid, which was slurried in cold methanol and recovered by filtration. It was washed with methanol (1 × 5 mL), ether (1 × 5 mL), and pentane (2 × 5 mL), then dissolved in acetone (5 mL) and filtered through Celite. The product was crystallized by vapor diffusion of diethyl ether into the acetone solution. The molecular rectangle was recovered by filtration and was washed with diethyl ether (1 × 5 mL) and pentane (2 × 3 mL). Yield = 0.296 g (91%). ^{1}H NMR ([D_6]acetone, 27 °C, 500 MHz): δ = 1.42 (s, 36 H), 2.84 (t, J = 6.55 Hz, 8 H), 3.10 (t, J = 6.61 Hz, 8 H), 7.23 (d, J = 1.68 Hz, 4 H), 7.65 (t, J = 1.63 Hz, 2 H), 7.68 (d, J = 7.86 Hz, 4 H), 7.86 (t, J = 6.63 Hz, 8 H), 8.02 (d, J = 5.05 Hz, 8 H), 8.14 (dd, J_1 = 1.80 Hz, J_2 = 7.75 Hz, 4 H), 8.65–8.68 (m, 16 H), 8.96 (d, J = 7.95 Hz, 8 H), 9.29 (s, 8 H), 9.36 (d, J = 1.67 Hz, 4 H), 9.65 (d, J = 6.46 Hz, 8 H) ppm. $C_{130}H_{126}F_{48}N_{18}Pt_4Sb_8$ (4847.04): calcd. C 37.17, H 2.62, N 5.20; found C 37.46, H 2.69, N 5.06. ESI-MS: a series of peaks were observed that were consistent with $[M - n(SbF_6)]^{n+}$ (n = 2–6): for example, 571.5 [**10** – 6(SbF_6)]$^{6+}$, 733.2 [**10** – 5(SbF_6)]$^{5+}$, 975.0 [**10** – 4(SbF_6)]$^{4+}$, 1379.1 [**10** – 3(SbF_6)]$^{3+}$, 2187.8 [**10** – 2(SbF_6)]$^{2+}$.

Pt Molecular Rectangle Formed with 4,4′-Dipyridylethane (11): A procedure analogous to that above was used. One equivalent of 4,4′-dipyridylethane (0.025 g, 0.135 mmol) was added to the dry acetone solution formed after the reaction of $AgSbF_6$ with [Pt(COD)I_2], and the reaction mixture was heated at reflux (70 °C). The mixture was stirred at this temperature for 2 d. The solvent was removed under reduced pressure to yield a yellow solid, which was slurried in cold methanol and recovered by filtration. It was washed with methanol (1 × 5 mL), ether (1 × 5 mL), and pentane (2 × 5 mL), then dissolved in acetone (5 mL) and filtered through Celite. The product was crystallized by vapor diffusion of diethyl ether into the acetone solution. The molecular rectangle was recovered by filtration and was washed with diethyl ether (1 × 5 mL) and pentane (2 × 3 mL). Yield = 0.290 g (76%). ^{1}H NMR ([D_6] acetone, 27 °C, 500 MHz): δ = 1.42 (s, 36 H), 2.86 (t, J = 6.83 Hz, 8 H), 3.10 (t, J = 6.44 Hz, 8 H), 3.51 (s, 8 H), 7.23 (d, J = 1.65 Hz, 4 H), 7.66 (t, J = 1.69 Hz 2 H), 7.70 (d, J = 7.80 Hz, 4 H), 7.97–8.00 (m, 8 H), 8.07–8.10 (m, 20 H), 8.25 (dd, J_1 = 1.80 Hz, J_2 = 7.75 Hz, 4 H), 8.60–8.65 (m, 8 H), 8.98 (d, J = 8.06 Hz, 8 H), 9.27 (d, J = 6.43 Hz, 4 H), 9.34 (s, 8 H), 9.42 (d, J = 1.89 Hz, 4 H). $C_{154}H_{134}F_{48}N_{18}Pt_4Sb_8$ (4903.15): calcd. C 37.72, H 2.75, N 5.14; found C 37.42, H 2.49, N 5.05. ESI-MS: a series of peaks were observed that were consistent with $[M - n(SbF_6)]^{n+}$ (n = 2–6): for example, 581.8 [**11** – 6(SbF_6)]$^{6+}$, 745.5 [**11** – 5(SbF_6)]$^{5+}$, 990.3 [**11** – 4(SbF_6)]$^{4+}$, 1399.1 [**11** – 3(SbF_6)]$^{3+}$, 2216.3 [**11** – 2(SbF_6)]$^{2+}$.

Host–Guest Interaction of Receptor 9 with 5: The procedure for stoichiometry determination employed for the host–guest adduct formed between **9** and **5** is representative. A series of solutions of **9** (1.75 mM) in dry [D_7]DMF containing varying amounts of **5** (0.23 mM to 11.4 mM) were prepared and were examined by ^{1}H NMR spectroscopy (60 °C). The host in [D_7]DMF solution is orange, as is the guest. The host–guest mixtures vary in color from orange-red to deep red (Figure 5). The mol ratio method[12] was applied, and the stoichiometry of the association was found to be one guest molecule per one host molecule (Figure 6). The data were analyzed using a curve-fitting procedure,[6] and K_1 was found to be 3670 ± 560 M^{-1}. ESI-MS ([D_7]DMF): a series of peaks were observed that were consistent with $[M - n(SbF_6)]^{n+}$ and $[M{\cdot}G - n(SbF_6)]^{n+}$ (n = 1–4): for example, 370.2 [**9** – 4(SbF_6)]$^{4+}$, 476.6 [**9·5** – 4(SbF_6)]$^{4+}$, 572.3 [**9** – 3(SbF_6)]$^{3+}$, 713.1 [**9·5** – 3(SbF_6)]$^{3+}$, 976.0 [**9** – 2(SbF_6)]$^{2+}$, 1188.4 [**9·5** – 2(SbF_6)]$^{2+}$ (Figure 7).

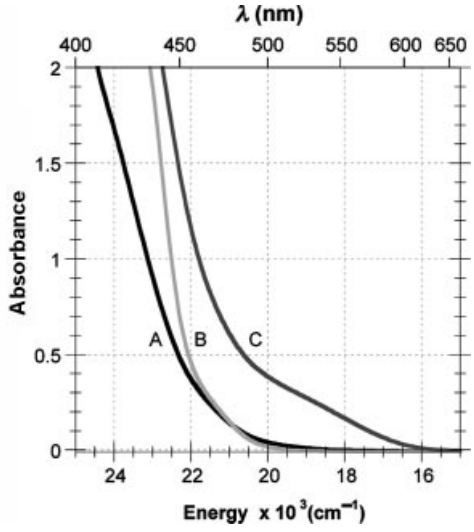

Figure 5. Absorption spectra for **9** (A, 1.75 mM), **5** (B, 2.05 mM), and a 1:1 solution (C) of **9** (1.75 mM) and **5** (1.89 mM). The experiments were performed at 25 °C in dry DMF.

Host–Guest Interaction of Receptor 9 with 6: The procedure was analogous to that used above. The stoichiometry of the association was found to be one guest molecule per one host molecule (Supporting Information). K_1 was found to be 1160 ± 210 M^{-1}. ESI-MS ([D_7]DMF): a series of peaks were observed that were consistent with $[M - n(SbF_6)]^{n+}$ and $[M{\cdot}G - n(SbF_6)]^{n+}$ (n = 1–4): for example, 370.2 [**2** – 4(SbF_6)]$^{4+}$, 467.1 [**9·6** – 4(SbF_6)]$^{4+}$, 572.3 [**9** – 3(SbF_6)]$^{3+}$, 701.5 [**9·6** – 3(SbF_6)]$^{3+}$, 976.0 [**9** – 2(SbF_6)]$^{2+}$, 1170.3 [**9·6** – 2(SbF_6)]$^{2+}$.

Host–Guest Interaction of Molecular Rectangle 10 with 5: The procedure for stoichiometry determination employed for the host–guest adduct formed between **10** and **5** is representative. A series of solutions of **10** (1.65 mM) in dry [D_7]DMF containing varying amounts of **5** (0.25 mM to 23.4 mM) were prepared and were examined by ^{1}H NMR spectroscopy (60 °C). The host in [D_7]DMF solution is orange, as is the guest. The host–guest mixtures vary in

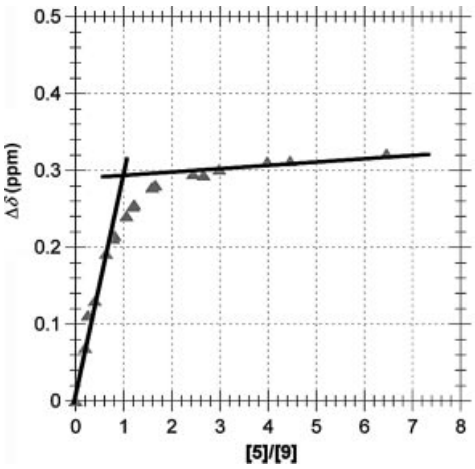

Figure 6. ^{1}H NMR stoichiometry titration for the host–guest complex formed between **9** and **5**. The experiments were performed at 60 °C in [D_7]DMF. The concentration of **9** was held constant at 1.75 mM, and the concentration of **5** was varied between 0.23 mM and 11.4 mM. The plot refers to the proton H_h (see Scheme 2).

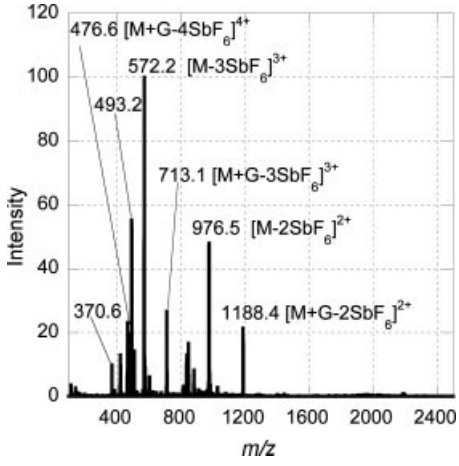

Figure 7. ESI-MS (DMF, 1.75 mM) of the host–guest complex formed between **9** and **5**, *m*/*z* = 370.6 [**9** – 4SbF_6]$^{4+}$, 476.6 [**9·5** – 4SbF_6]$^{4+}$, 572.3 [**9** – 3SbF_6]$^{3+}$, 713.1 [**9·5** – 3SbF_6]$^{3+}$, 976.5 [**9** – 2SbF_6]$^{2+}$, 1188.4 [**9·5** – 2SbF_6]$^{2+}$.

color from orange-red to deep red (Figure 8). The stoichiometry of the association was found to be two guest molecules per one host molecule (Figure 9). Equilibrium constants were determined using a previously described algorithm.[9] The microscopic value of K_1 was found to be 4100 ± 400 M^{-1}, and K_2 was 4200 ± 200 M^{-1}. K_2/K_1 = 1.02. ESI-MS ([D_7]DMF): a series of peaks were observed that were consistent with [M – *n*(SbF_6)]$^{n+}$, [M·G – *n*(SbF_6)]$^{n+}$ and [M·2G – *n*(SbF_6)]$^{n+}$ (*n* = 2–5): for example, 733.1 [**10** – 5(SbF_6)]$^{5+}$, 975.7 [**10** – 4(SbF_6)]$^{4+}$, 1081.3 [**10·5** – 4(SbF_6)]$^{4+}$, 1187.4 [**10**–(**5**)$_2$ – 4(SbF_6)]$^{4+}$, 1379.4 [**10** – 3(SbF_6)]$^{3+}$, 1520.7 [**10·5** – 3(SbF_6)]$^{3+}$, 1662.3 [**10**–(**5**)$_2$ – 3(SbF_6)]$^{3+}$, 2187.5 [**10** – 2(SbF_6)]$^{2+}$ (Figure 10).

Host–Guest Interaction of Molecular Rectangle 11 with 5: The procedure was analogous to that used above. The stoichiometry of the association was found to be two guest molecules per one host molecule (Supporting Information). K_1 was found to be 3800 ± 300 M^{-1}, and K_2 was 4400 ± 200 M^{-1}. K_2/K_1 = 1.15. ESI-MS ([D_7]DMF): a series of peaks were observed that were consistent with [M – *n*(SbF_6)]$^{n+}$, [M·G – *n*(SbF_6)]$^{n+}$ and [M·2G – *n*(SbF_6)]$^{n+}$ (*n* = 2–5): for example, 744.5 [**11** – 5(SbF_6)]$^{5+}$, 990.4 [**11** – 4(SbF_6)]$^{4+}$, 1095.4 [**11·5** – 4(SbF_6)]$^{4+}$, 1201.4 [**11**–(**5**)$_2$ – 4(SbF_6)]$^{4+}$, 1398.2 [**11** – 3(SbF_6)]$^{3+}$, 1539.2 [**11·5** – 3(SbF_6)]$^{3+}$, 1680.7 [**11**–(**5**)$_2$ – 3(SbF_6)]$^{3+}$, 2215.6 [**11** – 2(SbF_6)]$^{2+}$, 2428.1 [**11**–(**5**)$_2$ – 2(SbF_6)]$^{2+}$ (Supporting Information).

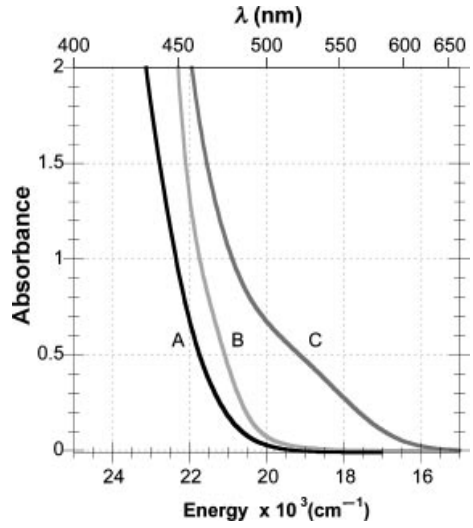

Figure 8. Absorption spectra for **10** (A, 1.65 mM), **5** (B, 3.45 mM), and a 1:2 solution (C) of **10** (1.65 mM) and **5** (3.55 mM). The experiments were performed at 25 °C in dry DMF.

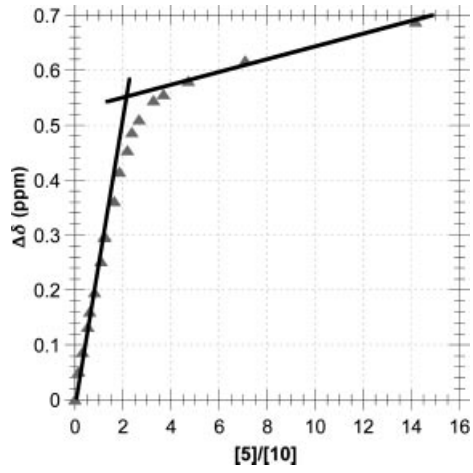

Figure 9. ^{1}H NMR stoichiometry titration for the host–guest complex formed between **10** and **5**. The experiments were performed at 60 °C in [D_7]DMF. The concentration of **10** was held constant at 1.65 mM, and the concentration of **5** was varied between 0.25 mM and 23.4 mM. The plot refers to the proton H_h (see Scheme 2).

Host–Guest Interaction of Molecular Rectangle 10 with 6: The procedure was analogous to those described above. The stoichiometry of the association was found to be two guest molecules per one host molecule (Supporting Information). K_1 was found to be 1450 ± 200 M^{-1}, and K_2 was 5200 ± 400 M^{-1}. K_2/K_1 = 3.58. ESI-MS ([D_7]DMF): a series of peaks were observed that were consistent with [M – *n*(SbF_6)]$^{n+}$ and [M·2G – *n*(SbF_6)]$^{n+}$ (*n* = 3–5): for example, 888.1 [**10**–(**6**)$_2$ – 5(SbF_6)]$^{5+}$, 975.4 [**10** – 4(SbF_6)]$^{4+}$, 1169.2 [**10**–(**6**)$_2$ – 4(SbF_6)]$^{4+}$, 1379.3 [**10** – 3(SbF_6)]$^{3+}$, 1638.0 [**10**–(**6**)$_2$ – 3(SbF_6)]$^{3+}$, 2186.9 [**10** – 2(SbF_6)]$^{2+}$ (Supporting Information).

Host–Guest Interaction of Molecular Rectangle 11 with 6: The procedure was analogous to those described above. The stoichiometry of the association was found to be two guest molecules per one

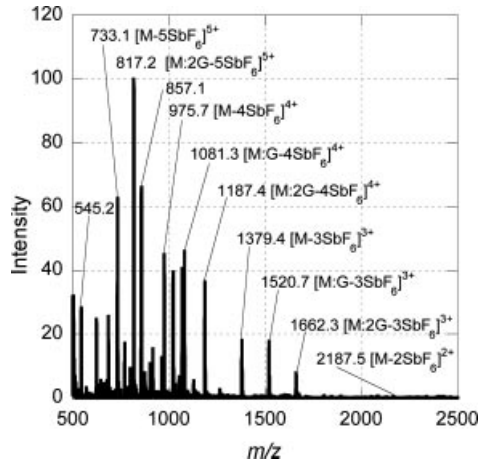

Figure 10. ESI-MS (DMF, 1.65 mM) of the host–guest complex formed between **10** and **5**, 733.1 [**10** – 5(SbF_6)]$^{5+}$, 975.7 [**10** – 4(SbF_6)]$^{4+}$, 1081.3 [**10·5** – 4(SbF_6)]$^{4+}$, 1187.4 [**10**–(**5**)$_2$ – 4(SbF_6)]$^{4+}$, 1379.4 [**10** – 3(SbF_6)]$^{3+}$, 1520.7 [**10·5** – 3(SbF_6)]$^{3+}$, 1662.3 [**10**–(**5**)$_2$ – 3(SbF_6)]$^{3+}$, 2187.5[**10** – 2(SbF_6)]$^{2+}$.

host molecule (Supporting Information). K_1 was found to be 1250 ± 200 M^{-1}, and K_2 was 5600 ± 400 M^{-1}. K_2/K_1 = 4.58. ESI-MS ([D_7]DMF): a series of peaks were observed that were consistent with [M – n(SbF_6)]$^{n+}$, [M·G – n(SbF_6)]$^{n+}$ and [M·2G – n(SbF_6)]$^{n+}$ (n = 3–5): for example, 710.2 [**11**–(**6**)$_2$ – 6(SbF_6)]$^{6+}$, 744.5 [**11** – 5(SbF_6)]$^{5+}$, 929.1 [**11**–(**6**)$_2$ + 2DMF – 5(SbF_6)]$^{5+}$, 990.1 [**11** – 4(SbF_6)]$^{4+}$, 1026.9 [**11** + 2DMF – 4(SbF_6)]$^{4+}$, 1086.4 [**11·6** – 4(SbF_6)]$^{4+}$, 1183.3 [**11**–(**6**)$_2$ – 4(SbF_6)]$^{4+}$, 1398.2 [**11** – 3(SbF_6)]$^{3+}$, 2215.6 [**11** – 2(SbF_6)]$^{2+}$ (Supporting Information).

Host–Guest Interaction of Molecular Rectangle 10 with 7: The procedure was analogous to that used above. The mol ratio method[12] was applied, and the stoichiometry of the association was found to be four guest molecules per one host molecule (Supporting Information). Because of the high host–guest stoichiometry, the binding constants could not be determined. ESI-MS ([D_7]DMF): a series of peaks were observed that were consistent with [M – n(SbF_6)]$^{n+}$(n = 2–6): for example, 571.5 [**10** – 6(SbF_6)]$^{6+}$, 733.2 [**10** – 5(SbF_6)]$^{5+}$, 975.0 [**10** – 4(SbF_6)]$^{4+}$, 1379.1 [**10** – 3(SbF_6)]$^{3+}$, 2187.8 [**10** – 2(SbF_6)]$^{2+}$. No peaks due to the host–guest adducts were observed (Supporting Information).

Crystallographic Structural Determination for the Host–Guest Adduct Formed from 10 and 5: Crystals of the complex were grown by dissolving a 1:2 mixture of host **10** and guest **5** in methyl ethyl ketone and vapor diffusing with methanol for seven days at –4 °C.

Data Collection: A red, brick-shaped fragment (0.20 × 0.15 × 0.15 mm) was selected under a stereomicroscope while immersed in Fluorolube oil to avoid possible reaction with air. The crystal was removed from the oil using a tapered glass fiber that also served to hold the crystal for data collection. The crystal was mounted and centered on a Bruker SMART APEX system at 100 K. Rotation and still images showed the diffractions to be sharp. Frames separated in reciprocal space were obtained and provided an orientation matrix and initial cell parameters. Final cell parameters were obtained from the full data set.

A "full sphere" data set was obtained which samples approximately all of the reciprocal space to a resolution of 0.84 Å using steps of 0.3° in ω and 30-s integration times for each frame. Data were collected at 100 K. Integration of intensities and refinement of cell parameters were performed with SAINT.[18] Absorption corrections were applied using SADABS[18] based on redundant diffractions.

Structure Solution and Refinement: The space group was determined as $P\bar{1}$ on the basis of systematic absences and intensity statistics. Patterson methods were used to locate some Pt atoms and repeated-difference Fourier maps allowed recognition of many carbon atoms. It soon became clear that the expected SbF_6 and other Pt atoms were either not located or located as split atoms. While the C units became obvious, considerable difficulties were encountered in locating some C atoms, particularly those associated with the split Pt atoms or in expected solvent. The F atoms of the SbF_6 groups were either not found or found with poor geometry. It was concluded that there is severe disorder for the anions, solvent, and guest Pt units. Sb and Pt guest positions were usually located and their occupancy refined. Some F atoms were assigned but in general SbF_6 units were not complete. Although anisotropic refinement for the C framework was possible, some terminal C atoms showed poor geometry. No H location was attempted. Final refinement was anisotropic for all C, N, and Pt atoms of the framework. Some thermal parameters were unusual, but overall the framework was consistent with that expected. All ORTEP diagrams have been drawn with 50% probability ellipsoids. The final R value of approximately 14% directly results from the inability to locate the anions and guest molecules.

The CIF file CCDC 267851 [for **10**–(**5**)$_2$] contains the supplementary crystallographic data for this paper. These data can be obtained free of charge from The Cambridge Crystallographic Data Centre via www.ccdc.cam.ac.uk/data_request/cif.

Supporting Information: The Supporting Information contains the ^{1}H NMR stoichiometry plots, ESI-MS, UV/Vis spectra, COSY, and NOESY spectra for the host–guest adducts.

Acknowledgments

This work was supported by grants from the Basic Sciences Division of the Department of Energy.

[1] a) J. Rebek, Jr., *Acc. Chem. Res.* **1984**, *17*, 258–264; b) S. Shinkai, M. Ikeda, A. Sugasaki, M. Takeuchi, *Acc. Chem. Res.* **2001**, *34*, 494–503; c) M. Takeuchi, M. Ikeda, A. Sugasaki, S. Shinkai, *Acc. Chem. Res.* **2001**, *34*, 865–873; d) L. Kovbasyuk, R. Krämer, *Chem. Rev.* **2004**, *104*, 3161–3187. e) Fujita invoked allosterism in the formation of a 1:4 host–guest complex, but this assertion was not supported by stability-constant data; D. Oguro, M. Miyazawa, H. Oka, K. Yamaguchi, K. Ogura, M. Fujita, *Nature* **1995**, *378*, 469–472.
[2] a) J. Rebek, Jr., J. E. Trend, R. V. Wattley, S. Chakravorti, *J. Am. Chem. Soc.* **1979**, *101*, 4333–4337; b) J. Rebek, Jr., R. V. Wattley, *J. Am. Chem. Soc.* **1980**, *102*, 4853–4854.
[3] C. A. Hunter, L. D. Sarson, *Angew. Chem.* **1994**, *106*, 2424–2426; *Angew. Chem. Int. Ed. Engl.* **1994**, *33*, 2313–2316.
[4] a) S.-Y. Chang, H.-Y. Jang, K.-S. Jeong, *Chem. Eur. J.* **2004**, *10*, 4358–4366; b) S.-Y. Chang, M.-C. Um, H. Uh, H.-Y. Jang, K.-S. Jeong, *Chem. Commun.* **2003**, *16*, 2026–2027.
[5] H. Kawai, R. Katoono, K. Nishimura, S. Matsuda, K. Fujiwara, T. Tsuji, T. Suzuki, *J. Am. Chem. Soc.* **2004**, *126*, 5034–5035.
[6] A. J. Goshe, I. M. Steele, B. Bosnich, *J. Am. Chem. Soc.* **2003**, *125*, 444–451.
[7] J. D. Crowley, A. J. Goshe, I. M. Steele, B. Bosnich, *Chem. Eur. J.* **2004**, *10*, 1944–1952.
[8] a) G. W. V. Cave, N. W. Alcock, J. P. Rourke, *Organometallics* **1999**, *18*, 1801–1803; b) G. W. V. Cave, F. P. Fanizzi, R. J. De-

eth, W. Errington, J. P. Rourke, *Organometallics* **2000**, *19*, 1355–1364.
[9] R. D. Sommer, A. L. Rheingold, A. J. Goshe, B. Bosnich, *J. Am. Chem. Soc.* **2001**, *123*, 3940–3952.
[10] A. J. Goshe, I. M. Steele, C. Ceccarelli, A. L. Rheingold, B. Bosnich, *Proc. Natl. Acad. Sci. USA* **2002**, *99*, 4823–4829.
[11] a) C. A. Schalley, T. Muller, P. Linnartz, M. Witt, M. Schafer, A. Lutzen, *Chem. Eur. J.* **2002**, *8*, 3538; b) C. A. Schalley, *Mass Spectrom. Rev.* **2001**, *20*, 253; c) C. A. Schalley, *Int. J. Mass Spectrom.* **2000**, *194*, 11.
[12] a) A. S. Meyer, G. H. Ayers, *J. Am. Chem. Soc.* **1957**, *79*, 49–53; b) H.-J. Schneider, *Principles and Methods in Supramolecular Chemistry*, John Wiley & Sons, New York, **2000**; c) H. Tsukube, H. Furuta, A. Odani, Y. Takeda, K. Yoshihiro, Y. Inoue, Y. Liu, H. Sakamoto and K. Kimura, *Comprehensive Supramolecular Chemistry* (Eds.: S. E. D. Davies, J. A. Ripmeester), Permagon, Oxford, UK, **1996**, vol. 8, p. 425.
[13] K. A. Connors, *Binding Constants*, John Wiley & Sons, New York, **1987**.
[14] D. Neuhaus, M. P. Williamson, *The Nuclear Overhauser Effect in Structural and Conformational Analysis*, 2nd ed., John Wiley and Sons, New York, **2000**.
[15] J. D. Crowley, I. M. Steele, B. Bosnich, *Inorg. Chem.* **2005**, *44*, 2989–2991.
[16] a) A. J. Goshe, B. Bosnich, *Synlett* **2001**, 941–944; b) J. D. Crowley, B. Bosnich, *Eur. J. Inorg. Chem.* **2005**, 2015–2025.
[17] a) A. J. Goshe, I. M. Steele, B. Bosnich, *Inorg. Chim. Acta* **2004**, *357*, 4544–4551; b) A. J. Goshe, J. D. Crowley, B. Bosnich, *Helv. Chim. Acta* **2001**, *84*, 2971–2985.
[18] G. Sheldrick, *SHELXTL* (version 6.1) Program Library, G. Bruker Analytical X-ray Systems, Madison, WI, **2000**.

Received: May 2, 2005
Published Online: August 4, 2005

